Flexible Framework for Lung and Colon Cancer Automated Analysis Across Multiple Diagnosis Scenarios

Marwen SAKLI[1], Chaker ESSID[2], Bassem BEN SALAH[3], Hedi SAKLI[4]
SERCOM Laboratory-Tunisia Polytechnic School, University of Carthage, La Marsa 2078, Tunisia[1, 2, 3]
FST, Campus Universitaire El-Manar, 2092 El Manar Tunis, Tunisia[2]
National Engineering School of Tunis-ENIT Communication Systems Research Laboratory SYSCOM-LR-99-ES21, University of Tunis El-Manar, Tunisia[4]
EITA Consulting, 7 Rue Du Chant Des Oiseaux, 78360 Montesson, France[4]

***Abstract*—Among humans, lung and colon cancers are regarded as primary contributors to mortality and morbidity. They may grow simultaneously in organs, having a harmful influence on the lives of people. If tumor is not diagnosed early, it is likely to spread to both of those organs. This research presents a flexible framework that employs lightweight Convolutional Neural Networks architecture for automating lung and colon cancer diagnosis in histological images across multiple diagnosis scenarios. The LC25000 dataset is commonly used for this task. It includes 25000 histopathological images belonging to 5 distinct classes, which are lung adenocarcinoma, lung squamous cell carcinoma, benign lung tissue, colon adenocarcinoma, and benign colonic tissue. This work includes three diagnosis scenarios: (S1) evaluates lung or colon samples, (S2) distinguishes benign from malignant images, and (S3) classifies images into five categories from the LC25000 dataset. Across all the scenarios, the scored accuracy, recall, precision, F1-score, and AUC exceeded 0.9947, 0.9947, and 0.9995, respectively. This investigation with a lightweight Convolutional Neural Network containing only 1.612 million parameters is extremely efficient for automated lung and colon cancer diagnosis, outperforming several current methods. This method might help doctors provide more accurate diagnoses and improve patient outcomes.**

Keywords*—Lung and colon cancers; histopathological images; LC25000 dataset; lightweight convolutional neural networks; multiple diagnosis scenarios

I. INTRODUCTION

Statistical analysis undertaken in the United States showed that lung and colon (LC) cancers are expected to be among the three most prevalent cancer types in 2020. Moreover, these malignancies were expected to have the most fatality rates of any cancer diagnosis. The GLOBOCAN 2020 data indicated LC cancer incidence rates of 11.4% and 18.0%, respectively [1]. The World Health Organization (WHO) anticipated that roughly 4 Million persons on a global scale will acquire lung or colon cancer in 2020, resulting in approximately 2.7 Million deaths. The presented information highlights the substantial worldwide health effects of lung and colon cancers. It is worth noting that LC cancers can coexist, with roughly 17% of cases containing both tumors concurrently [2].

Lung cancer, a malignant disease, arises from the excessive and unregulated multiplication of atypical cells within the lung [3]. This can result in tumor formation, which may spread to other parts of the body. Various factors play a role in the increasing incidence of lung cancer, including exposure to harmful substances, such as tobacco smoke, and aging. Early-stage lung cancer often presents with subtle or no symptoms, making early detection challenging [4]. Consequently, diagnosis frequently occurs at a late stage, when therapeutic options are curtailed. Adenocarcinoma and squamous cell carcinoma constitute the majority of lung cancer cases [5]. Adenocarcinoma, which can affect both smokers and non-smokers, is more prevalent in women and younger individuals It often originates in the outermost regions of the pulmonary tissue and can spread rapidly. Squamous cell carcinoma, primarily associated with smoking, can develop anywhere in the lungs and tends to grow and spread aggressively [6,7].

The causes of LC cancer are multiple and complex. Smoking is the main risk factor for lung cancer, while for colon cancer, a low-fiber diet, prolonged sedentary lifestyle obesity, and certain genetic factors can increase the risk of other environmental factors such as exposure to certain chemical substances or air pollution contribute in the multiplication of these cancers. It is crucial to note that these risk factors are not synonymous with inevitable cancer development, but adopting them can considerably increase the chances of developing these diseases.

Generally, to detect and diagnose cancer, a variety of diagnostic tests are employed, including imaging modalities such as Magnetic Resonance Imaging (MRI) [8-11], X-rays [12], CT scans, and dermoscopy [13-16], as well as tissue sampling procedures such as biopsies. Histological images offer considerable advantages over other types of medical imaging in the analysis and characterization of LC cancers. Histology enables microscopic analysis of tissues removed during biopsy or surgery. This enables us to observe cancer cells directly, and determine their type, stage, and aggressiveness. This information is crucial for making an accurate diagnosis, choosing the most appropriate treatment, and assessing prognosis. Additional imaging techniques, such as radiography, computed tomography, or MRIs, provide information on the anatomy and size of tumors but do not allow detailed analysis of

cellular characteristics. The microscopic examination of tissue parts by experienced pathologists is crucial for determining the presence of cancer cells and classifying their type and subtype [17,18]. Although, manual analysis of histopathological images consumes time. Also, it is labor-intensive and subjective process, prone to inter-observer variability. Pathologists may have differing interpretations of the same image, leading to potential diagnostic errors, especially when dealing with subtle morphological features. Additionally, the growing number of medical images and the complexity of certain cases further exacerbate the challenge.

To overcome these constraints [19], this work investigates the application of Deep Learning (DL) and machine learning (ML) approaches to automate cancer analysis in medical images [12,20]. DL techniques provide potential solutions to mitigate these challenges. Through the utilization of deep neural networks, DL models can process high quantities of histopathological images, learning to recognize complex characteristics and features associated with LC cancers. This can lead to improved diagnostic and efficiency and precision in comparison with traditional approaches.

This study tries to balance dependability as well as precision in LC cancer classification. The main contributions of this study include:

- Proving that DL approaches can effectively diagnose and analyze LC cancers.
- Employing a huge dataset of 25000 histopathological images to classify LC cancers.
- Illustrating three diagnosis scenarios to ensure the flexibility of the presented framework.
- Designing a lightweight CNN model with only 1.6 million parameters, assessing its performance, while comparing it to current approaches.
- Achieving accuracy, F1-score, and AUC over 99.47%, 99.47%, and 99.95%, respectively, throughout all analytic phases and diagnosis scenarios.
- Scoring F1-score and accuracy of 99.17% and 99.47%. Also, a sensitivity and specificity of 99.07%, and 99.65% across all classes of overall diagnosis scenarios, respectively.

This investigation employs a classification approach to analyze a dataset containing lung and colon cancer images. The subsequent sections of this investigation are organized as follows: the second section presents a review of pertinent literature. The third section delineates the proposed methodology. The fourth section provides a detailed performance evaluation of the presented lightweight CNN. The fifth section offers a thorough discussion of the findings. This paper will be ended by the last section, Section VI.

II. Related Work

This study contributes to the research effort aimed at improving diagnostic support for LC cancer using artificial intelligence techniques. A new method for diagnosing histopathological images on the LC25000 dataset [21], a reference in the field. Several academics have recently used this dataset to develop AI-based applications.

Sakr et al. [22] introduce a lightweight DL approach using a CNN for powerful categorization of cancer of the colon. Histopathological images were normalized before being processed by the CNN model. Across two classes, their proposed system attained a high accuracy of 99.50%. Using the same data, Hasan et al. [23] presented an innovative DL strategy for the automated identification of colon adenocarcinomas. Their approach involved a DCNN model, coupled with several image preprocessing techniques, to obtain meaningful features from digital histological images. The proposed system demonstrated impressive performance, achieving a maximum accuracy of 99.80% in differentiating between non-cancerous and cancerous tissues. For the same target, Gabralla et al [24] introduced a novel stacking-based deep learning framework. Their approach involved integrating multiple pre-trained CNN models (ResNet50 [25], DenseNet121 [26], InceptionV3, and VGG16 [27]) with a meta-learner. The meta-learner was trained to effectively combine the predictions of the individual models, resulting in a significant improvement in overall performance. The proposed method achieved an ideal score of 100% in terms of F1-score and accuracy, using the LC25000 dataset [21]. In addition, they attained F1-score and accuracy of 98% when employing the WCE dataset [28,29], surpassing the performance of the individual base models. To enhance the accuracy of colon cancer prediction, Di Giammarco et al. [30] employed different pre-trained models. The metrics of the proposed method was assessed on a sub-dataset of LC25000 comprising 10,000 colon images. The experimental results demonstrated that MobileNet [31] had the highest, f1-score, accuracy, recall, and precision of 99.9%, indicating the model's capability of the model to efficiently categorize colon issues.

Concerning lung cancer, Hatuwal and Thapa [32] aimed to classify three classes of tissue: benign, squamous cell carcinoma, and adenocarcinoma. A CNN approach was trained and validated on a sub-dataset of histological data, LC25000 dataset [21]. The model demonstrated strong performance, achieving an accuracy of 96.11% and 97.2%, during the training and validation phases. Nishio et al. [33] established a CAD system to automate the analysis of lung tissue in histological images. The system employed a multi-stage approach involving image feature extraction and ML classification. Two feature extraction techniques were investigated: conventional texture analysis (TA) and homology-based image processing (HI). Eight ML algorithms were trained and evaluated using the extracted features. The results found in the experiments demonstrated the higher efficiency of the HI-based approach over the TA-based system, achieving an accuracy of 99.33%. The study of Hamed et al. [34] is about a novel system for the rapid and precise classification of lung tissue histological data. The treated tissue types were only benign and squamous cell carcinoma. The proposed approach involves a two-stage process: feature extraction using a lightweight CNN model and classification using a LightGBM classifier. The CNN technique, designed with a minimal number of parameters, efficiently extracts discriminative features from the preprocessed images. Subsequently, the LightGBM classifier, leveraging multiple threads, effectively classifies the input data into various tissue

types. When evaluated on the LC25000 dataset, the approach achieved a remarkable accuracy of 99.6% and a sensitivity of 99.6%. To increase lung cancer classification accuracy, Noaman et al [35] propose a novel hybrid feature extraction technique where the powerful capabilities of charateristic extraction of DenseNet201 was combined with the complementary information provided by color histograms. A comprehensive evaluation of eight machine learning algorithms, including, SVM, MultinomialNB, LGBM, CatBoost, XGBoost, KNN, and RF, was conducted on the LC25000 dataset [21]. The outcomes demonstrate that the established hybrid feature set, when coupled with an appropriate ML algorithm, achieves a remarkable accuracy of 99.683%. To further validate the generalizability of our approach, we applied it to the task of the analysis of the breast cancer utilizing the images of the BreakHis dataset [36]. The model achieved a high accuracy of 94.808%, highlighting the advantage of their hybrid feature extraction technique for various medical image analysis tasks.

Several researchers tried to classify the whole of the five types of tissues figured in the LC25000 dataset [21]. In fact, Ali et al. [37] reached 99.04% and 99.58% as F1-score and accuracy LC cancer classification. They employed a multi-input dual-stream Capsule Network (CapsNet) [38]. It consists of two major blocks: Convolutional Layers Block (CLB) and Separable Convolutional Layers Block (SCLB). CLB and SCLB uses traditional and separable convolutional layers. The SCLB block takes uniquely preprocessed images using gamma correction and color balancing. Also, it takes multi-scale fusion and image sharpening. This dual-input approach enhances feature learning. Besides CapsNet, numerous works applied Efficient Networks (EfficientNets) [39] for LC cancer classification. Masud et al [40] present a novel DL-based framework for the diagnostic of five distinct classes of LC tissues, containing both benign and malignant conditions. By leveraging advanced digital image processing techniques and DL models, the proposed framework effectively extracts relevant features from histopathological images and accurately classifies them. Experimental results demonstrate that the developed tool can detect cancer tissues with a high accuracy and F1-score with values of 96.33% and 96.38%, respectively. In Mehmood et al.'s study [41], a pre-trained AlexNet was adapted for the task of histological image classification. The initial model, trained using a generic dataset, achieved promising results for most image classes, except for one class where the accuracy was relatively low. To address this issue, the simple and effective technique of contrast enhancement was applied to enhance the quality of images from the underperforming class. This targeted approach significantly boosted the overall accuracy of the model to 98.4% while maintaining computational efficiency. Attallah et al. [42] developed a novel framework that integrated DL and feature reduction techniques to ameliorate the accuracy of the classification of histopathology images. To extract relevant features, histopathology scans were processed using three models: ShuffleNet [43], MobileNet [31], and SqueezeNet [44]. The high-dimensional feature vectors obtained from these models are then subjected to Fast Walsh-Hadamard Transform (FWHT) and dimensionality reduction by the application of Principal Component Analysis (PCA). To further enhance feature representation, Discrete Wavelet Transform (DWT) was employed to combine the reduced characteristics from the three DL models. The resulting reduced and fused feature sets are subsequently passed into four different ML algorithms for classification. The established framework achieves F1-score and accuracy of 99.6% on the given dataset. The study of Al-Jabbar et al. [45] introduces three novel strategies for the early diagnostic of the lung cancer based on the LC25000 dataset. To enhance image quality and improve diagnostic accuracy, preprocessing techniques were applied to enhance the contrast of affected areas. Subsequently, high-dimensional patterns were determined using the VGG-19 [27] and GoogLeNet [46] models. To reduce dimensionality and retain crucial information, Principal Component Analysis (PCA) was employed. The first strategy involved training separate Artificial Neural Networks (ANN) models using the features extracted from VGG-19 and GoogLeNet. The other approach combined the patterns from both models before applying dimensionality reduction and ANN classification. The third strategy, which yielded the best performance, involved fusing the features extracted from VGG-19, GoogLeNet, and handcrafted characteristics before training the ANN model. This approach achieved a sensitivity, specificity, precision, accuracy, and AUC surpassing 99.64%. Kumar et al. [47] did a comparative analysis to measure the effectiveness of handcrafted and DL-based feature extraction techniques for LC cancer classification. In this research, six handcrafted pattern extraction methods were employed to capture color, texture, shape, and structural information from histopathological images. These handcrafted features were then used to train and evaluate 4 ML classifiers: Gradient Boosting, MLP, Random Forest, and SVM-RBF. In another approach, seven pre-trained DL models are utilized to determine high-level patterns from data. These deep features were subsequently fed into the same four ML classifiers. The findings demonstrated that the classification performance was significantly enhanced when using DL-based features compared to handcrafted features. Notably, the Random Forest categorizer combined with DenseNet-121 achieved the highest ROC-AUC, accuracy, and F1-score with values exceeding 91%. In Anjum et al's work [48] EfficientNet models (B0 to B7) [39] were applied for the diagnostic of LC cancer in histopathological data. To improve model performance and mitigate overfitting, transfer learning, and parameter tuning techniques were employed. After preprocessing the LC25000 dataset [21] to remove noise and standardize image formats, experiments were conducted using different image resolutions, ranging from 224x224 pixels to 600x600 pixels. The models were evaluated based on classification accuracy and loss. While all EfficientNet [39] variants achieved promising results, EfficientNetB2 demonstrated the highest performance, attaining an accuracy of 97.24% when trained on 260x260 pixel images.

Some studies did not concentrate on creating automated diagnostic approaches specifically for colon or lung, or lung and colon cancer. Rather, they developed methods that can comprehensively address the diagnosis of colon cancer, lung cancer, or both. The work of Talkuder et al. [49] identified efficiently LC cancers by the employment of a hybrid ensemble method. The proposed model integrates powerful feature extraction approaches with ensemble learning and high-performance filtering to effectively analyze histopathological images from the LC25000 dataset [21]. The results demonstrate the superior performance of their hybrid model, reaching

accuracies of 100%, 99.05%, and 99.30% for colon, lung, and combined LC cancer classification, respectively. In the research of Hage Chehade et al. [50], they aimed to develop a computerized diagnostic system capable of efficiently categorizing the five distinct classes of LC tissues, including two types of colon cancer and three categories of lung cancer. When leveraging ML techniques, feature engineering, and image processing methods, meaningful information was extracted from histopathological data. The LC25000 dataset [21] was utilized to train and evaluate five ML models: Random Forest, XGBoost, SVM, Multilayer Perceptron, and Linear Discriminant Analysis. The best results were obtained using XGBoost. For colon cancer, they reached accuracy and F1-score of 99.3% and 99.5%, respectively. Concerning lung cancer, the accuracy, precision, recall, and F1-score reached were 99.53%, 99.33%, 99.33%, and 99.33%, respectively. Also, for LC cancer, they got an accuracy of 99%, precision of 98.6%, recall of 99%, and F1-score of 98.8%.

This work aims to develop a flexible based on multi-scenario diagnosis for LC cancer automated analysis. This framework is based on a lightweight CNN and uses the LC25000 dataset to evaluate its performance in this task. For the first scenario, a method was developed to detect if the input image corresponds to a lung or a colon. The results were perfect since all the performance metrics had attained 100%. Based on this result, two methods were established. The first approach is dedicated to determining the nature of the colon tissue type. Its AUC, F1-score, and accuracy reached 100%. The second method aims to classify lung cancer. It got AUC, F1-score, and accuracy with values of 99. 95%, 99.47%, and 99. 47%, respectively. The target of the second scenario is LC malignancy detection in histological images. This approach scored perfect AUC, F1-score, and accuracy with values of 100%, respectively. The purpose of the third scenario is to classify the totality of LC tissue types. AUC, F1-score, and accuracy achieved values of 99.96%, 99.76%, and 99.76%, respectively. Table I presents the description of the cited methods from the literature and the proposed approaches.

III. Proposed Method

In this study, three diagnosis scenarios are presented. The first scenario (S1) is composed of two distinct stages: the initial stage (S1-1) aims to evaluate whether the input image corresponds to either a lung or colon sample. Based on the outcome of this stage, the second stage (S1-2) is designed to determine the specific class associated with the identified organ. In the second scenario (S2), the target is to identify whether the input data belongs to either the benign or malignant class, irrespective of its origin. The third scenario (S3) involves categorizing the input data among all the type of the tissues (5 classes) of LC25000 dataset. Fig. 1 illustrates an overview of the three scenarios presented. Fig. 2 presents the workflow of the presented strategies of analysis.

A. Dataset

This investigation uses the LC25000 dataset [21], which includes 25000 histopathological images whose size is 768x768 pixels in JPEG format. This dataset is an invaluable resource for training and assessing ML models in cancer diagnosis, particularly for LC cancer. The dataset is distributed across five classes: lung squamous cell carcinoma (lung_scc), lung adenocarcinoma (lung_aca), benign lung tissue (lung_n), benign colonic tissue(colon_n), and colon adenocarcinoma (colon_aca). It was methodically obtained from an initial pool of 750 HIPAA-compliant and verified data, which included 250 cases of each class. Then, it was subsequently augmented using the Augmentor software where the used techniques are random horizontal/vertical flips and left/right rotations (higher than 25 degrees). Consequently, the number of images was enlarged to 25000 and 5000 histopathological images per class.

B. Data Preparation

This section is reserved to detail the data preparation steps, including data pre-processing and data splitting.

1) Data Pre-processing: This step is about resizing images from the original shape to (64, 64, 3). Then, for each scenario, the images belonging to the appropriate classes were selected.

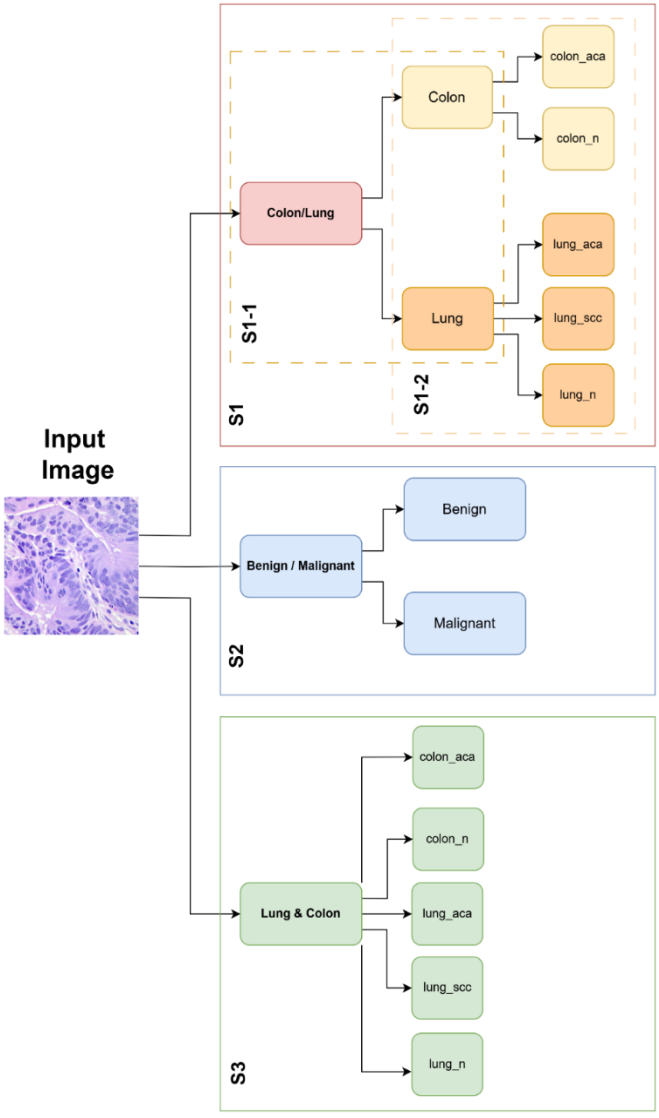

Fig. 1. Synoptic of the three scenarios presented.

TABLE I. STATE-OF-THE-ART AND PROPOSED METHODS DESCRIPTION

Method	Year	Organ	classes	Params(M)	Description	Accuracy
[33]	2021	Lung	3	-	- Image Feature Extraction: HI, TA, Multiscale Analysis - ML Models: KNN, SVM, DT, RF…	0.9933
[40]	2021	LC	5	-	- Digital Image Processing (DIP) - CNN	0.9633
[37]	2021	LC	5	-	- Image Preprocessing: Color Balancing, Image Sharpening, Gamma Correction, and Multi-Scale Fusion. - Multi-Input Capsule Network. - Dual-Input Learning.	0.9958
[50]	2022	Lung Colon LC	3 2 5	-	- Feature Engineering: texture, shape, color histograms… - Image Processing: image normalization, noise removal, and contrast enhancement. -ML Models: XGBoost, SVM, RF, LDA…	0.9953 0.993 0.99
[42]	2022	LC	5	-	- DL models: ShuffleNet, MobileNet, SqueezeNet. - Feature Reduction: PCA, FHWT - Feature Fusion: Discrete Wavelet Transform (DWT) - ML Algorithms: SVM, RF, KNN, LR	0.9960
[23]	2022	Colon	2	-	- Digital Image Processing: Noise reduction, data normalization - Deep CNN	0.9980
[47]	2022	LC	5	-	- Handcrafted Feature Extraction: color, texture, shape, and structure - Deep Feature Extraction: Transfer Learning models - Classifiers: GB, SVM-RBF, MLP, RF	0.9860
[49]	2022	Lung Colon LC	3 2 5	-	-Hybrid Ensemble Feature Extraction strategy: Deep Feature Extraction using DL models and integration of multiple classifiers. - High-Performance Filtering for enhancing image features	0.9905 1.0000 0.9930
[22]	2022	Colon	2	4.6	- Image Preprocessing: Image normalization - DL Model: Convolutional Neural Networks (CNNs)	0.9950
[41]	2022	LC	5	-	- Image Preprocessing: Contrast enhancement. - DL Model: Fine-tuned AlexNet (a pretrained CNN model).	0.984
[34]	2023	Lung	2	-	- Image Preprocessing: Data normalization, resizing, and potentially other enhancements. - Deep Feature Extraction: Convolutional Neural Networks (CNNs) for feature extraction. - ML Models: LightGBM for classification of extracted features.	0.996
[48]	2023	LC	5	9.2	- Image Preprocessing: Image cleaning, resizing, and normalization. - Transfer Learning: EfficientNet and its variants (B0 to B7) for image classification. - Parameter Tuning	0.9724
[45]	2023	LC	5	-	- Deep Features Extraction: GoogLeNet and VGG-19 for highlighting characteristics. - Dimensionality Reduction: PCA - Feature Fusion: Combining features from different models VGG-19 and GoogLeNet, and handcrafted patterns. - Classifier: Artificial Neural Network (ANN)	0.9964
[24]	2023	Colon	2	-	- Ensemble Learning: Stacking DL models to combine predictions from multiple base models. - Pretrained CNNs: InceptionV3, ResNet50, VGG16, DenseNet121 for feature extraction and initial predictions. - Meta-learner: Combined prediction based on SVM and base models. - Explainable AI (XAI)	1.0000
[30]	2024	Lung	3	-	- Deep Learning: CNN - Explainable AI (XAI)	0.999
[35]	2024	Lung	3		- Deep Features extraction: DenseNet201 - Image Preprocessing: Color Histogram Technique. - ML Algorithms: SVM, MultinomialNB, LGBM, CatBoost, XGBoost, KNN, RF	**0.9968**
Proposed Methods	2024	Lung Colon LC LC	3 2 2 5	1.6	- Image Preprocessing: Resizing - DL Models: Lightweight CNN	0.9947 **1.0000** **1.0000** **0.9976**

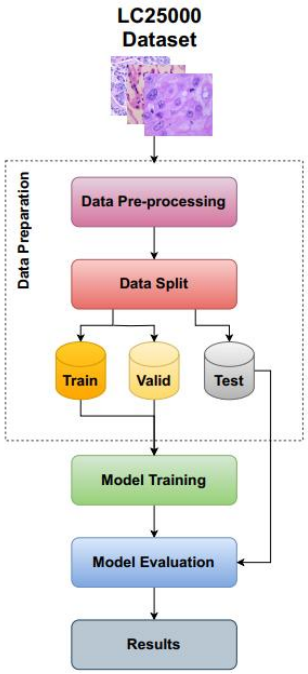

Fig. 2. Workflow of the proposed methods.

2) Data split: DL studies often divide the totality of the data into three sets which are training set, validation set, and testing set. The training set determines model parameters, whereas the validation set adjusts hyperparameters and measures overall performance. The testing dataset measures the model's effectiveness using previously unknown data. The LC25000 dataset was partitioned into training and validation subsets, and also a test set, with an 80:20 split.

The training and validation sets were partitioned using a 90:10 ratio.

C. Model

The proposed model's design belongs to CNN architecture. It consists of two main components: the Features Extractor (FE) and the Classifier. The input data (histological images) will be transformed by FE to advanced characteristics that identify shapes and correlations. This is achieved by the use of three repetitious blocks, including Convolution (Conv2D) and Max Pooling (MaxPool2D) bidimensional layers. The repeated blocks consist of four layers: 2 Conv2D, MaxPool2D, and Batch Normalization (BN). The extracted characteristics will be turned by the classifier to predicted labels of classes. It comprises Dense, Dropout, and Flatten layers, and 4x repeated blocks. The repeated blocks consist of BN and Dense layers. The designed lightweight CNN is depicted in Fig. 3.

D. Hyperparameters

For the training process, this research uses the trial-and-error process to determine the most optimal method. The model's input parameters were set at (64, 64, 3), matching the dimensions of the given image. 32 was the set batch size. The optimal number of epochs (ep) was 50. Adam which has a learning rate of 1.10-3 was the employed optimizer. In addition, the categorical cross-entropy loss was utilized as a loss function. During training, a learning rate schedule was used to manage this phase. It was set as follows:

$$lr = \begin{cases} lr, & ep \leq 10 \\ lr.\exp(-10^{-1}), & ep > 10 \end{cases} \quad (1)$$

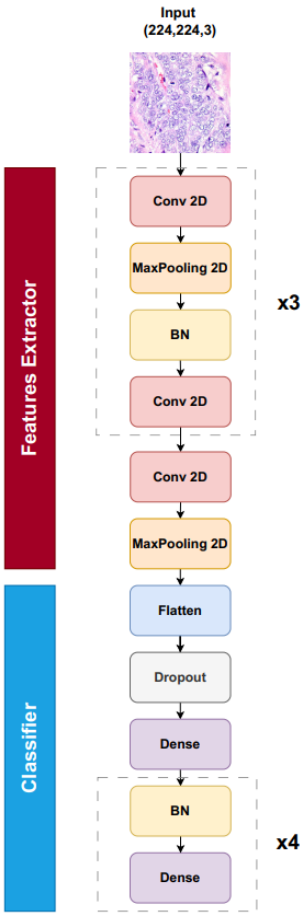

Fig. 3. Architecture of the proposed lightweight CNN.

E. Metrics

The proposed methods were evaluated using different metrics such as AUC, accuracy, F1 score, and. AUC calculates the ability of the system to differentiate between positive and negative data. F1-score incorporates precision and recall into a one statistic. Finally, Accuracy is the proportion of correct predictions to total calculated by the model.

IV. Results

This section is dedicated to show the experiment results. The training phases were done on a personal computer with 16GB of NVIDIA T4 x 2 GPU, 30GB of RAM, and a CPU of 2.20 GHz Intel Xeon. The goal of this research is to provide a versatile framework based on multi-scenario for automated LC cancer analysis. This paragraph aims to present the results for each diagnosis scenario.

1) Diagnosis Scenario (S1): The first scenario (S1) consists of two dependent stages: the first stage (S1-1) determines whether the input image refers to lung or colon data. Based on the results of this stage, the second stage (S1-2) is meant to

determine the exact class corresponding to the indicated organ Table II represents the results of the proposed system during the diagnosis scenarios S1-1, S1-2 Colon, and S1-2 Lung in the training, validation, and test phases. In fact, for scenario S1-1, the AUC F1-score, and accuracy of the established method reached 1.0000 in all phases. This perfect result enables us to pass to the second level of the actual scenario. Regarding the second level, scenario S1-2 Colon, the proposed model attained the same efficiency excluding the loss. Concerning the diagnosis scenario S1-2 Lung, the AUC, F1-score, and accuracy exceeded 0.9947 in the totality of phases.

TABLE II. RESULTS OF THE PROPOSED METHOD DURING THE DIAGNOSIS SCENARIOS S1-1, S1-2 COLON, AND S1-2 LUNG IN THE TRAINING, VALIDATION, AND TEST PHASES

	S1-1			**S1-2 Colon**			**S1-2 Lung**		
Phase	Train	Valid	Test	Train	Valid	Test	Train	Valid	Test
Accuracy	1.0000	1.0000	1.0000	1.0000	1.0000	1.0000	1.0000	0.9983	0.9947
F1-Score	1.0000	1.0000	1.0000	1.0000	1.0000	1.0000	1.0000	0.9983	0.9947
AUC	1.0000	1.0000	1.0000	1.0000	1.0000	1.0000	1.0000	1.0000	0.9995

In this study, the classification metrics were also presented for the classes. The proposed approach reached an accuracy, sensitivity, specificity, and F1-score, of 1.000 for both the colon and lung classes. Moreover, in the S1-2 Colon, the previous metrics scored a value of 1.0000. Furthermore, for the S1-2 Lung, with the designed LWCNN, accuracy and F1-score surpassed 0.9947 and 0.9917, while the specificity and sensitivity, each exceeded, 0.9954 and 0.9907, respectively. Table III illustrates the results of the proposed method across all classes during the diagnosis scenarios S1-1, S1-2 Colon, and S1-2 Lung.

These highly performant results can be confirmed by the confusion matrixes. Fig. 4(a), (b), and (c) depict the confusion matrix of the presented scenarios S1-1, S1-2 Lung, and S1-2 Colon, respectively. This indicates that the proposed LWCNN can not only properly identify instances belonging to their respective classes but also successfully separate them from other classes, resulting in no substantial confusion or misclassification. For the S1-2 Lung, the proposed model's confusion matrix is nearly ideal.

TABLE III. RESULTS OF THE PROPOSED METHOD ACROSS ALL CLASSES DURING THE DIAGNOSIS SCENARIOS S1-1, S1-2 COLON, AND S1-2 LUNG

	Class	**Accuracy**	**F1-score**	**Se**	**Sp**
S1-1	Lung	1.0000	1.0000	1.0000	1.0000
	Colon	1.0000	1.0000	1.0000	1.0000
S1-2 Lung	lung_aca	0.9947	0.9923	0.9933	0.9954
	lung_scc	0.9947	0.9917	0.9907	0.9965
	lung_n	1.0000	1.0000	1.0000	1.0000
S1-2 Colon	colon_aca	1.0000	1.0000	1.0000	1.0000
	colon_n	1.0000	1.0000	1.0000	1.0000

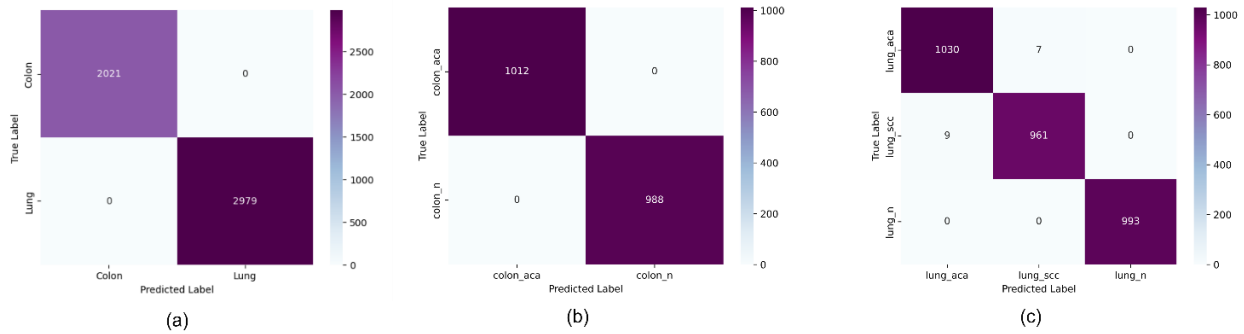

Fig. 4. Confusion matrices of presented LWCNN for diagnosis scenarios: (a) S1-1, (b) S1-2 Colon, and (c) S1-2 Lung.

Similar findings were observed through the ROC (Receiver Operating Characteristic) curve, which illustrates the balance between the true positive rate (TPR) and the false positive rate (FPR) at varying classification levels. As the curve approaches the plot's top-left corner, the model's efficiency improves. Fig. 5(a), (b), and (c) illustrate the ROC curves for the three diagnostic scenarios. In the lung and colon classification (S1-1), the curve attained a point at (0,1), indicating 0% false positives and 100% true positives. The same result was observed for colon classification in S1-2 Colon, confirming an AUC value of 1.0000 for the studied classes. For the S1-2 Lung scenario, the ROC curve was very near to the top-left corner, with AUC values for the lung class above 0.9999.

Overall, the proposed method is efficient for the diagnosis scenario (S1). This was confirmed by a batch of images randomly chosen from the test set for each diagnosis sub-scenario. Fig. 6 depicts the reel test using random test images. All input test images were correctly predicted with a confidence rate higher than 99.99%.

2) Diagnosis Scenario (S2): The second scenario (S2) is designed to find out whether the input data is attributed to the

malignant or benign class, irrespective of its origin (lung or colon). Table IV presents the outcomes for this scenario across the training, validation, and testing phases. The designed LWCNN achieved flawless performance in this scenario, with accuracy, F1-score, and AUC all reaching 1.0000 across every phase.

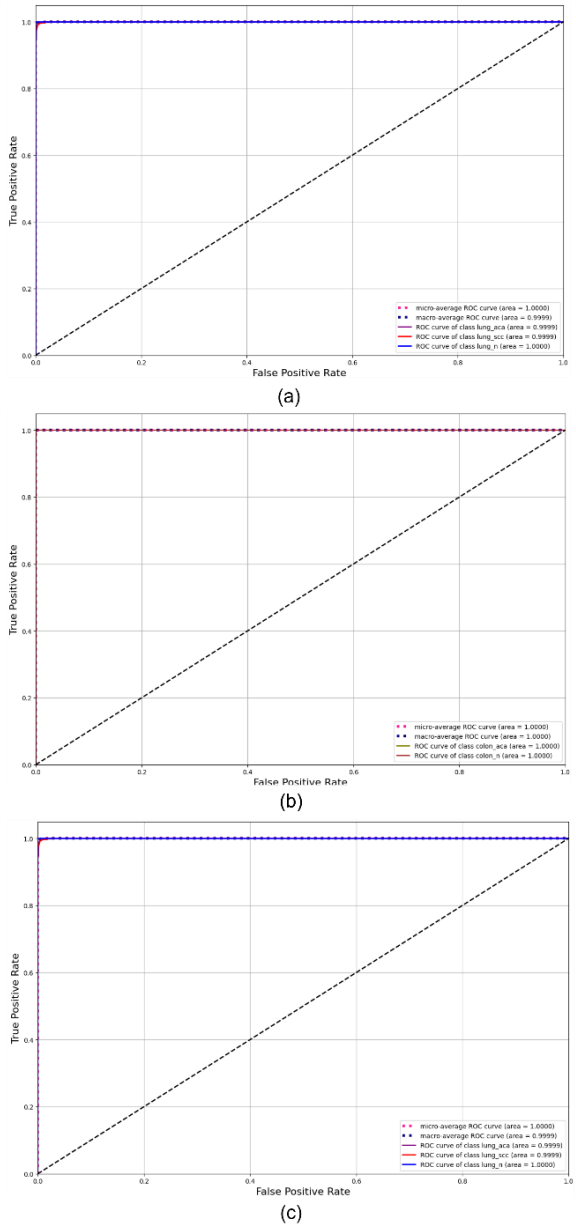

Fig. 5. ROC curves for diagnosis scenarios: (a) S1-1, (b) S1-2 Colon, and (c) S1-2 Lung.

TABLE IV. PROPOSED APPROACH'S FINDINGS DURING THE DIAGNOSIS SCENARIO (S2) IN THE TRAINING, VALIDATION, AND TEST PHASES

Phase	Training	Validation	Test
Accuracy	1.0000	1.0000	1.0000
F1-Score	1.0000	1.0000	1.0000
AUC	1.0000	1.0000	1.0000

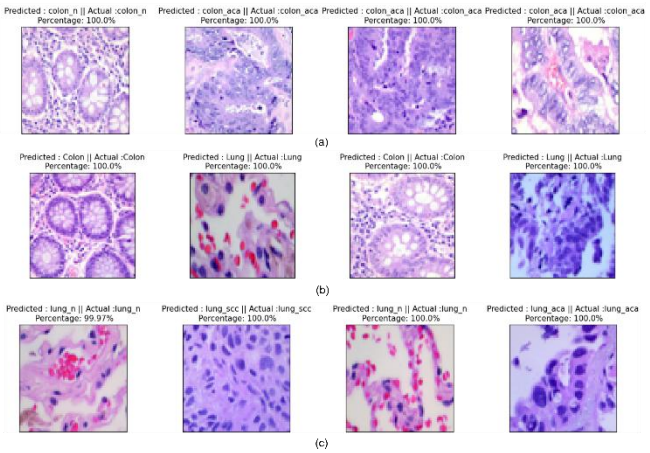

Fig. 6. Framework Test images arbitrarily selected from the test data used for the diagnosis of the sub-scenarios: (a) S1-1, (b) S1-2 Lung, and (c) S1-2 Colon.

This shows that it was capable to consistently and perfectly differentiate between malignant and benign classes with perfect precision, recall, and overall classification metrics.

The classification metrics for each class (benign and malignant) further confirm this outstanding performance. In all phases, the proposed approach attained a sensitivity, specificity, F1-score, and an accuracy of 1.0000 for both classes. These results suggest that the model not only accurately identified instances as either benign or malignant but also demonstrated exceptional sensitivity in detecting positive cases and specificity in ruling out negatives, leading to no false positives or false negatives. The results of the proposed method across all classes during the diagnosis scenario (S2) in Table V.

The confusion matrix, depicted in Fig. 7, provides further validation of the model's perfect performance. Both matrices reveal zero false positives and false negatives, indicating that the LWCNN model accurately classified all instances without any misclassification. This underscores the model's robustness in distinguishing between benign and malignant cases with absolute accuracy.

Moreover, the ROC curves for scenario (S2), illustrated in Fig. 8, also demonstrate the exceptional performance of the LWCNN model. The ROC curve reaches the top-left corner, signifying 0% false positives and 100% true positives for both benign and malignant classifications. This results in an AUC value of 1.0000, confirming that the model performed optimally across all thresholds.

In conclusion, the results of scenario S2 demonstrate the effectiveness of the presented method in discriminating between malignant and benign cases with 100% accuracy. This finding is further corroborated by a set of arbitrarily selected images from the test set, all of which were correctly classified with a confidence rate exceeding 99.99%. Fig. 9 illustrates these perfect predictions, further demonstrating the reliability of the model in real diagnostic applications.

3) Diagnosis Scenario (S3): The third scenario (S3) addresses the categorization of treated images to one of the five available categories from LC25000 dataset. Table VI

summarizes the results of this scenario across all phases. The described LWCNN model demonstrated strong performance, achieving accuracy, F1-score, and AUC values ranging between 0. 9976 and 1.0000, depending on the specific class and phase. While some variations in performance were observed, the model consistently classified the majority of images with high precision and reliability across all phases.

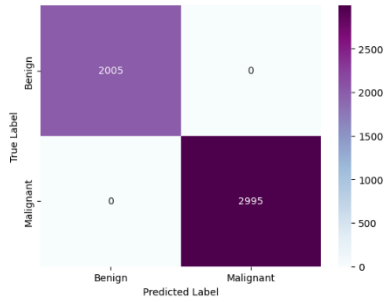

Fig. 7. Confusion matrix of presented LWCNN for diagnosis scenario (S2).

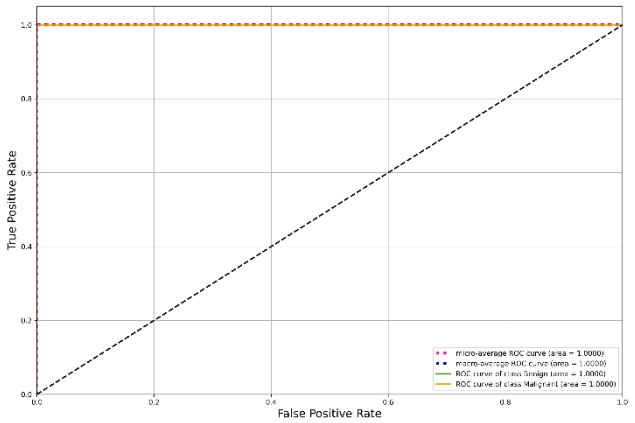

Fig. 8. ROC curves for diagnosis scenario (S2).

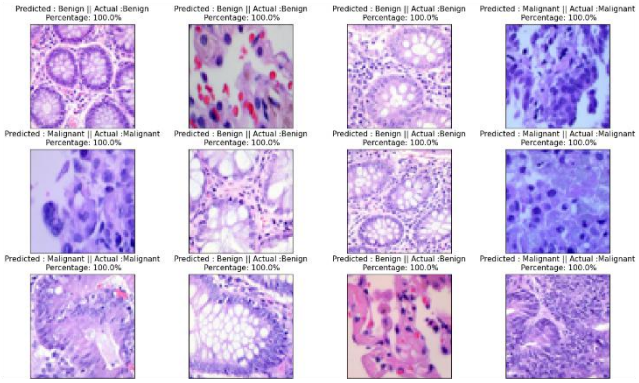

Fig. 9. Framework Test images arbitrarily selected from the test data used for the diagnosis scenario (S2).

TABLE V. RESULTS OF THE PROPOSED METHOD ACROSS ALL CLASSES DURING THE DIAGNOSIS SCENARIO (S2)

Class	Accuracy	F1-score	Se	Sp
Benign	1.0000	1.0000	1.0000	1.0000
Malignant	1.0000	1.0000	1.0000	1.0000

TABLE VI. PROPOSED APPROACH'S FINDINGS DURING THE DIAGNOSIS SCENARIO (S3) IN THE TRAINING, VALIDATION, AND TEST PHASES

Phase	Training	Validation	Test
Accuracy	1.0000	0.9970	0.9976
F1-Score	1.0000	0.9970	0.9976
AUC	1.0000	0.9991	0.9996

TABLE VII. RESULTS OF THE PROPOSED METHOD ACROSS ALL CLASSES DURING THE DIAGNOSIS SCENARIO (S3)

Class	Accuracy	F1-score	Se	Sp
colon_aca	0.9996	0.9990	0.9990	0.9998
colon_n	0.9996	0.9990	0.9990	0.9998
lung_aca	0.9980	0.9949	0.9949	0.9988
lung_scc	0.9980	0.9949	0.9949	0.9987
lung_n	1.0000	1.0000	1.0000	1.0000

A detailed examination of the classification metrics reveals that the model achieved near-perfect results in several classes, with accuracy, F1-score, sensitivity, and specificity reaching values as high as 1.0000 for the lung_n class. In other classes, the performance remained highly competitive, with these metrics exceeding 0.9949. This demonstrates the robustness of the model in handling multiple classification tasks while maintaining substantial accuracy. Table VII demonstrates the results of the proposed method across all classes during the diagnosis scenario (S3).

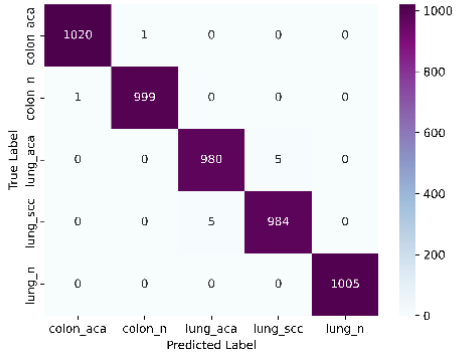

Fig. 10. Confusion matrix of presented LWCNN for the diagnosis scenario (S3).

Fig. 10 illustrates the confusion matrix for the five classes, further validating the model's efficacy in scenario (S3). While some minor misclassifications occurred, indicated by a low value of FP and FN, the overall confusion matrix reveals that the LWCNN model effectively distinguished between the five classes with minimal error, maintaining a high level of classification accuracy.

The ROC curves for scenario (S3), shown in Fig. 11, further support the model's effectiveness. Across all categories, the ROC curve closely approaches the top-left corner. This demonstrates the outstanding capability of the presented approach to distinguish between positive and negative cases. The corresponding AUC values exceed 0.9999, confirming the

model's high sensitivity and specificity across multiple thresholds.

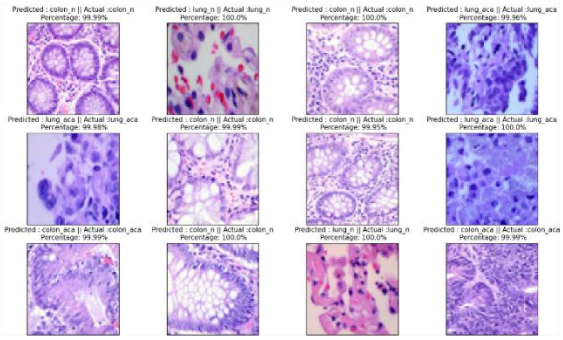

Fig. 11. ROC curves for diagnosis scenario (S3).

In conclusion, the third scenario (S3) demonstrates that the proposed method is highly performant in categorizing input data into one of the five LC25000 dataset classes, with results consistently ranging between 99% and 100%. Despite the minor variations in performance across classes, the model exhibited reliable classification capabilities. Fig. 12 displays randomly selected test images, which were classified with a confidence rate exceeding 99%, further confirming the model's potential in practical diagnostic tasks.

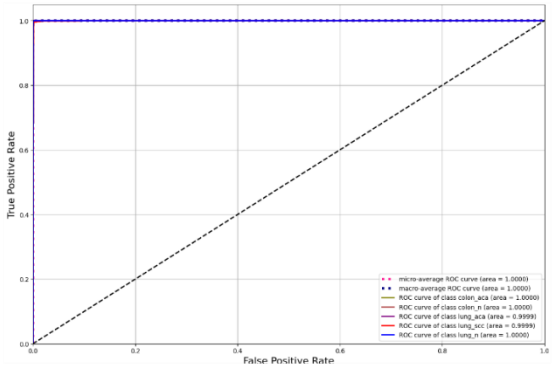

Fig. 12. Framework Test images arbitrarily selected from the test data used for the diagnosis scenario (S3).

V. Discussion

This section is dedicated to debate the experiment results, and compare them to existing approaches. Table VIII illustrates a comparative analysis of the performances of the presented approaches against a selection of well-established ML and DL-based systems for LC cancer classification, as detailed in Section II. Similarly, all the selected literature strategies which employed LC25000 dataset when assessing the outcomes of their models.

TABLE VIII. Comparison of the Overall Findings of the Presented Approaches and the Literature Approaches

Method	Year	Organ	Classes	Parameters (M)	Accuracy	F1-Score	AUC
[33]	2021	Lung	3	-	0.9933	-	-
[40]	2021	LC	5	-	0.9633	0.9638	-
[37]	2021	LC	5	-	0.9958	0.9904	-
[50]	2022	Lung Colon LC	3 2 5	-	0.9953 0.993 0.99	0.9933 0.995 0.988	-
[42]	2022	LC	5	-	0.9960	0.9960	-
[23]	2022	Colon	2	-	0.9980	0.9980	-
[47]	2022	LC	5	-	0.9860	0.9850	-
[49]	2022	Lung Colon LC	3 2 5	-	0.9905 1.0000 0.9930	-	-
[22]	2022	Colon	2	4.6	0.9950	0.9849	-
[41]	2022	LC	5	-	0.984	-	-
[34]	2023	Lung	2	-	0.996	**0.996**	-
[48]	2023	LC	5	9.2	0.9724	-	-
[45]	2023	LC	5	-	0.9964	-	0.998
[24]	2023	Colon	2	-	1.0000	1.0000	-
[30]	2024	Colon	2	-	0.999	0.999	0.998
[35]	2024	Lung	3		**0.9968**	-	-
Proposed Methods	2024	Lung Colon LC LC	3 2 2 5	**1.6**	0.9947 **1.0000** **1.0000** **0.9976**	0.9947 **1.0000** **1.0000** **0.9976**	**0.9995** **1.0000** **1.0000** **0.9996**

This research introduces a flexible framework for automatic analysis of LC cancer. The performance obtained highlights its robustness and efficiency. In fact, the used model was a lightweight CNN, which has a minimalist total number of parameters, 1.6 million parameters, when compared to those of Sakr et al [22] and Anjum et al. [48] where the total parameter is 4.6 and 9.2 million parameters, respectively. The comparison will cover three developed methods, which are colon cancer

classification, lung cancer classification, and LC classification. In colon classification, the proposed method reached the top efficiency with 100% AUC, F1-score, and accuracy. Equally, Gabralla et al. [24] attained the same performance. However, the authors used a more complex model with two levels, which contained individual models and stacking models.

In addition, they used more data preprocessing steps. For example, they applied common data augmentation (DA) like rotating, rescaling, zooming etc. In LC classification, the proposed method reaches an accuracy, F1-score, and AUC of 0.9947, 0.9947, and 0.9995, respectively. This performance is higher than those of Nishio et al. [33], and Talukder et al.'s [49] methods. Although it is very slightly lower than those of Masud et al. [40], Hage Chehad et al. [50], Hamed et al. [34], and Noaman et al.'s [35] approaches. Hamed et al. [34] worked only on two tissue types and not on the totality of the presented lung tissue types. In LC cancer classification, the proposed method outperformed all the cited approaches having the same task. The accuracy scored 0.9976. The F1-score reached 0.9976. The AUC attained 0.9996. These results demonstrate the model's remarkable accuracy, precision, recall, and discriminative power. Thus, the proposed approach is superior in terms of performance, lower in terms of complexity, and more recommended in terms of flexibility and practical usability, highlighting its suitability for this task at hand.

VI. Conclusion

This work aims to build a flexible framework based on multi-scenario diagnosis for LC cancers automated analysis. This was ensured by the employment of a lightweight CNN architecture with a small parameters number against other studies. In fact, the number of parameters was 1.612 million parameters. It was assessed using the LC25000 dataset which comprises five LC tissue types. The presented approach includes three diagnosis scenarios. The first diagnosis scenario (S1) is composed of two distinct stages: the initial stage (S1-1) aims to evaluate whether the input image corresponds to either a lung or colon sample. Based on the outcome of this stage, the second stage (S1-2) is designed to determine the specific class associated with the identified organ. In the second scenario (S2), the aim is to identify whether the input image belongs to either the benign or malignant class, irrespective of its origin. The third scenario (S3) involves categorizing the introduced image into one of the predefined categories in the LC25000 dataset. In the totality of these scenarios, the accuracy, F1-score, and AUC exceeded 0.9947. Regarding these metrics for each class in the presented scenarios, they were higher than 0.9907. The findings of this investigation highlight the important advantages of using the proposed method for the analysis of LC cancer. The model's improved accuracy, dependability, accessibility, flexibility, and capacity for continual development provide major benefits to improving patient care and outcomes. Upcoming work efforts should concentrate on analyzing the performance of the proposed technique over a variety of LC datasets, as well as expanding its assessment to other medical image modalities, such as radiographic or pathological imaging, in addition to histological images. This will assist to demonstrate its resilience, adaptability, and application in a variety of clinical contexts. Furthermore, future research should focus on demonstrating its use in real-world clinical settings to assure its widespread acceptance, generalizability, and potential to enhance diagnostic accuracy and patient outcomes.

References

[1] H. Sung et al., "Global Cancer Statistics 2020: GLOBOCAN Estimates of Incidence and Mortality Worldwide for 36 Cancers in 185 Countries," CA. Cancer J. Clin., vol. 71, no. 3, pp. 209–249, May 2021, doi: 10.3322/caac.21660.

[2] K. Kurishima et al., "Lung cancer patients with synchronous colon cancer," Mol. Clin. Oncol., vol. 8, no. 1, pp. 137–140, Jan. 2018, doi: 10.3892/mco.2017.1471.

[3] R. C. Callaghan, P. Allebeck, and A. Sidorchuk, "Marijuana use and risk of lung cancer: a 40-year cohort study," Cancer Causes Control, vol. 24, no. 10, pp. 1811–1820, Oct. 2013, doi: 10.1007/s10552-013-0259-0.

[4] M. M. Koo et al., "Presenting symptoms of cancer and stage at diagnosis: evidence from a cross-sectional, population-based study," Lancet Oncol., vol. 21, no. 1, pp. 73–79, Jan. 2020, doi: 10.1016/S1470-2045(19)30595-9.

[5] W. Zhou et al., "Causal relationships between body mass index, smoking and lung cancer: Univariable and multivariable Mendelian randomization," Int. J. Cancer, vol. 148, no. 5, pp. 1077–1086, 2021, doi: 10.1002/ijc.33292.

[6] K. Liu, X. Ning, and S. Liu, "Medical Image Classification Based on Semi-Supervised Generative Adversarial Network and Pseudo-Labelling," Sensors, vol. 22, no. 24, Art. no. 24, Jan. 2022, doi: 10.3390/s22249967.

[7] T. Khan et al., "Autophagy modulators for the treatment of oral and esophageal squamous cell carcinomas," Med. Res. Rev., vol. 40, no. 3, pp. 1002–1060, 2020, doi: 10.1002/med.21646.

[8] D. Daye et al., "Quantitative tumor heterogeneity MRI profiling improves machine learning–based prognostication in patients with metastatic colon cancer," Eur. Radiol., vol. 31, no. 8, pp. 5759–5767, Aug. 2021, doi: 10.1007/s00330-020-07673-0.

[9] M. Sakli, C. Essid, B. B. Salah, and H. Sakli, "Deep Learning Methods for Brain Tumor Segmentation," in Machine Learning and Deep Learning Techniques for Medical Image Recognition, CRC Press, 2023.

[10] E. Bębas et al., "Machine-learning-based classification of the histological subtype of non-small-cell lung cancer using MRI texture analysis," Biomed. Signal Process. Control, vol. 66, p. 102446, Apr. 2021, doi: 10.1016/j.bspc.2021.102446.

[11] M. C. Comes et al., "Early prediction of neoadjuvant chemotherapy response by exploiting a transfer learning approach on breast DCE-MRIs," Sci. Rep., vol. 11, no. 1, p. 14123, Jul. 2021, doi: 10.1038/s41598-021-93592-z.

[12] A. Souid, N. Sakli, and H. Sakli, "Classification and Predictions of Lung Diseases from Chest X-rays Using MobileNet V2," Appl. Sci., vol. 11, no. 6, Art. no. 6, Jan. 2021, doi: 10.3390/app11062751.

[13] M. Sakli, C. Essid, B. Ben Salah, and H. Sakli, "Skin Lesion Segmentation Using U-Net With Different Backbones: Comparative Study," in 2023 IEEE Afro-Mediterranean Conference on Artificial Intelligence (AMCAI), Dec. 2023, pp. 1–4. doi: 10.1109/AMCAI59331.2023.10431489.

[14] M. Sakli, C. Essid, B. B. Salah, and H. Sakli, "Lightweight CNN Towards Skin Lesions Automated Diagnosis In Dermoscopic Images," in 2023 International Conference on Innovations in Intelligent Systems and Applications (INISTA), Sep. 2023, pp. 1–6. doi: 10.1109/INISTA59065.2023.10310480.

[15] M. Sakli, C. Essid, B. Ben Salah, and H. Sakli, "Deep Learning-Based Multi-Stage Analysis for Accurate Skin Cancer Diagnosis using a Lightweight CNN Architecture," in 2023 International Conference on Innovations in Intelligent Systems and Applications (INISTA), Sep. 2023, pp. 1–6. doi: 10.1109/INISTA59065.2023.10310615.

[16] M. Sakl, C. Essid, B. B. Salah, and H. Sakli, "DL Methods for Skin Lesions Automated Diagnosis In Smartphone Images," in 2023 International Wireless Communications and Mobile Computing (IWCMC), Jun. 2023, pp. 1142–1147. doi: 10.1109/IWCMC58020.2023.10183254.

[17] K.-H. Yu et al., "Predicting non-small cell lung cancer prognosis by fully automated microscopic pathology image features," Nat. Commun., vol. 7, no. 1, p. 12474, Aug. 2016, doi: 10.1038/ncomms12474.

[18] W. D. Travis et al., "International Association for the Study of Lung Cancer/American Thoracic Society/European Respiratory Society International Multidisciplinary Classification of Lung Adenocarcinoma," J. Thorac. Oncol., vol. 6, no. 2, pp. 244–285, Feb. 2011, doi: 10.1097/JTO.0b013e318206a221.

[19] AM. Toğaçar, "Disease type detection in lung and colon cancer images using the complement approach of inefficient sets," Comput. Biol. Med., vol. 137, p. 104827, Oct. 2021, doi: 10.1016/j.compbiomed.2021.104827.

[20] M. Sakli, N. Sakli, and H. Sakli, "ECG Images Automated Diagnosis based on Machine Learning Algorithms," in 2023 20th International Multi-Conference on Systems, Signals & Devices (SSD), Feb. 2023, pp. 934–939. doi: 10.1109/SSD58187.2023.10411169.

[21] A. A. Borkowski, M. M. Bui, L. B. Thomas, C. P. Wilson, L. A. DeLand, and S. M. Mastorides, "Lung and Colon Cancer Histopathological Image Dataset (LC25000)," Dec. 16, 2019, arXiv: arXiv:1912.12142. doi: 10.48550/arXiv.1912.12142.

[22] A. S. Sakr, N. F. Soliman, M. S. Al-Gaashani, P. Pławiak, A. A. Ateya, and M. Hammad, "An Efficient Deep Learning Approach for Colon Cancer Detection," Appl. Sci., vol. 12, no. 17, Art. no. 17, Jan. 2022, doi: 10.3390/app12178450.

[23] M. I. Hasan, M. S. Ali, M. H. Rahman, and M. K. Islam, "Automated Detection and Characterization of Colon Cancer with Deep Convolutional Neural Networks," J. Healthc. Eng., vol. 2022, no. 1, p. 5269913, 2022, doi: 10.1155/2022/5269913.

[24] L. A. Gabralla et al., "Automated Diagnosis for Colon Cancer Diseases Using Stacking Transformer Models and Explainable Artificial Intelligence," Diagnostics, vol. 13, no. 18, Art. no. 18, Jan. 2023, doi: 10.3390/diagnostics13182939.

[25] K. He, X. Zhang, S. Ren, and J. Sun, "Deep Residual Learning for Image Recognition," in 2016 IEEE Conference on Computer Vision and Pattern Recognition (CVPR), Jun. 2016, pp. 770–778. doi: 10.1109/CVPR.2016.90.

[26] G. Huang, Z. Liu, L. Van Der Maaten, and K. Q. Weinberger, "Densely Connected Convolutional Networks," in 2017 IEEE Conference on Computer Vision and Pattern Recognition (CVPR), Jul. 2017, pp. 2261–2269. doi: 10.1109/CVPR.2017.243.

[27] K. Simonyan and A. Zisserman, "Very Deep Convolutional Networks for Large-Scale Image Recognition," Apr. 10, 2015, arXiv: arXiv:1409.1556. doi: 10.48550/arXiv.1409.1556.

[28] K. Pogorelov et al., "KVASIR: A Multi-Class Image Dataset for Computer Aided Gastrointestinal Disease Detection," in Proceedings of the 8th ACM on Multimedia Systems Conference, in MMSys'17. New York, NY, USA: Association for Computing Machinery, Jun. 2017, pp. 164–169. doi: 10.1145/3083187.3083212.

[29] J. Silva, A. Histace, O. Romain, X. Dray, and B. Granado, "Toward embedded detection of polyps in WCE images for early diagnosis of colorectal cancer," Int. J. Comput. Assist. Radiol. Surg., vol. 9, no. 2, pp. 283–293, Mar. 2014, doi: 10.1007/s11548-013-0926-3.

[30] M. Di Giammarco, F. Martinelli, A. Santone, M. Cesarelli, and F. Mercaldo, "Colon cancer diagnosis by means of explainable deep learning," Sci. Rep., vol. 14, no. 1, p. 15334, Jul. 2024, doi: 10.1038/s41598-024-63659-8.

[31] M. Sandler, A. Howard, M. Zhu, A. Zhmoginov, and L.-C. Chen, "MobileNetV2: Inverted Residuals and Linear Bottlenecks," in 2018 IEEE/CVF Conference on Computer Vision and Pattern Recognition, Jun. 2018, pp. 4510–4520. doi: 10.1109/CVPR.2018.00474.

[32] B. K. H. Thapa Himal Chand, "Lung Cancer Detection Using Convolutional Neural Network on Histopathological Images," Seventh Sense Research Group. Accessed: Oct. 27, 2024. [Online]. Available: https://dev.ijcttjournal.org//archives/ijctt-v68i10p104

[33] M. Nishio, M. Nishio, N. Jimbo, and K. Nakane, "Homology-Based Image Processing for Automatic Classification of Histopathological Images of Lung Tissue," Cancers, vol. 13, no. 6, Art. no. 6, Jan. 2021, doi: 10.3390/cancers13061192.

[34] E. A.-R. Hamed, M. A.-M. Salem, N. L. Badr, and M. F. Tolba, "An Efficient Combination of Convolutional Neural Network and LightGBM Algorithm for Lung Cancer Histopathology Classification," Diagnostics, vol. 13, no. 15, Art. no. 15, Jan. 2023, doi: 10.3390/diagnostics13152469.

[35] N. F. Noaman, B. M. Kanber, A. A. Smadi, L. Jiao, and M. K. Alsmadi, "Advancing Oncology Diagnostics: AI-Enabled Early Detection of Lung Cancer Through Hybrid Histological Image Analysis," IEEE Access, vol. 12, pp. 64396–64415, 2024, doi: 10.1109/ACCESS.2024.3397040.

[36] F. A. Spanhol, L. S. Oliveira, C. Petitjean, and L. Heutte, "A Dataset for Breast Cancer Histopathological Image Classification," IEEE Trans. Biomed. Eng., vol. 63, no. 7, pp. 1455–1462, Jul. 2016, doi: 10.1109/TBME.2015.2496264.

[37] M. Ali and R. Ali, "Multi-Input Dual-Stream Capsule Network for Improved Lung and Colon Cancer Classification," Diagnostics, vol. 11, no. 8, Art. no. 8, Aug. 2021, doi: 10.3390/diagnostics11081485.

[38] S. Sabour, N. Frosst, and G. E. Hinton, "Dynamic Routing Between Capsules," Nov. 07, 2017, arXiv: arXiv:1710.09829. doi: 10.48550/arXiv.1710.09829.

[39] M. Tan and Q. V. Le, "EfficientNet: Rethinking Model Scaling for Convolutional Neural Networks," Sep. 11, 2020, arXiv: arXiv:1905.11946. doi: 10.48550/arXiv.1905.11946.

[40] M. Masud, N. Sikder, A.-A. Nahid, A. K. Bairagi, and M. A. AlZain, "A Machine Learning Approach to Diagnosing Lung and Colon Cancer Using a Deep Learning-Based Classification Framework," Sensors, vol. 21, no. 3, Art. no. 3, Jan. 2021, doi: 10.3390/s21030748.

[41] S. Mehmood et al., "Malignancy Detection in Lung and Colon Histopathology Images Using Transfer Learning With Class Selective Image Processing," IEEE Access, vol. 10, pp. 25657–25668, 2022, doi: 10.1109/ACCESS.2022.3150924.

[42] O. Attallah, M. F. Aslan, and K. Sabanci, "A Framework for Lung and Colon Cancer Diagnosis via Lightweight Deep Learning Models and Transformation Methods," Diagnostics, vol. 12, no. 12, Art. no. 12, Dec. 2022, doi: 10.3390/diagnostics12122926.

[43] X. Zhang, X. Zhou, M. Lin, and J. Sun, "ShuffleNet: An Extremely Efficient Convolutional Neural Network for Mobile Devices," in 2018 IEEE/CVF Conference on Computer Vision and Pattern Recognition, Jun. 2018, pp. 6848–6856. doi: 10.1109/CVPR.2018.00716.

[44] F. N. Iandola, S. Han, M. W. Moskewicz, K. Ashraf, W. J. Dally, and K. Keutzer, "SqueezeNet: AlexNet-level accuracy with 50x fewer parameters and <0.5MB model size," Nov. 04, 2016, arXiv: arXiv:1602.07360. doi: 10.48550/arXiv.1602.07360.

[45] M. Al-Jabbar, M. Alshahrani, E. M. Senan, and I. A. Ahmed, "Histopathological Analysis for Detecting Lung and Colon Cancer Malignancies Using Hybrid Systems with Fused Features," Bioengineering, vol. 10, no. 3, Art. no. 3, Mar. 2023, doi: 10.3390/bioengineering10030383.

[46] C. Szegedy et al., "Going deeper with convolutions," in 2015 IEEE Conference on Computer Vision and Pattern Recognition (CVPR), Jun. 2015, pp. 1–9. doi: 10.1109/CVPR.2015.7298594.

[47] N. Kumar, M. Sharma, V. P. Singh, C. Madan, and S. Mehandia, "An empirical study of handcrafted and dense feature extraction techniques for lung and colon cancer classification from histopathological images," Biomed. Signal Process. Control, vol. 75, p. 103596, May 2022, doi: 10.1016/j.bspc.2022.103596.

[48] S. Anjum et al., "Lung Cancer Classification in Histopathology Images Using Multiresolution Efficient Nets," Comput. Intell. Neurosci., vol. 2023, no. 1, p. 7282944, 2023, doi: 10.1155/2023/7282944.

[49] Md. A. Talukder, Md. M. Islam, M. A. Uddin, A. Akhter, K. F. Hasan, and M. A. Moni, "Machine learning-based lung and colon cancer detection using deep feature extraction and ensemble learning," Expert Syst. Appl., vol. 205, p. 117695, Nov. 2022, doi: 10.1016/j.eswa.2022.117695.

[50] A. Hage Chehade, N. Abdallah, J.-M. Marion, M. Oueidat, and P. Chauvet, "Lung and colon cancer classification using medical imaging: a feature engineering approach," Phys. Eng. Sci. Med., vol. 45, no. 3, pp. 729–746, Sep. 2022, doi: 10.1007/s13246-022-01139-x..